The Astrophysical Journal Letters, 946:L44 (9pp), 2023 April 1 https://doi.org/10.3847/2041-8213/acc531

Evolution of Magnetic Field Fluctuations and Their Spectral Properties within the Heliosphere: Statistical Approach

Jana Šafránková[1], Zdeněk Němeček[1], František Němec[1], Daniel Verscharen[2], Timothy S. Horbury[3], Stuart D. Bale[4], and Lubomír Přech[1]
[1] Charles University, Faculty of Mathematics and Physics, V Holešovičkách 2, 180 00 Prague 8, Czech Republic; jana.safrankova@mff.cuni.cz
[2] Mullard Space Science Laboratory, University College London, Dorking, UK
[3] Imperial College London, Blackett Laboratory, South Kensington, London, UK
[4] University of California, Berkeley, CA, USA
Received 2023 February 6; revised 2023 February 28; accepted 2023 March 16; published 2023 April 5

Abstract

We present the first comprehensive statistical study of the evolution of compressive and noncompressive magnetic field fluctuations in the inner heliosphere. Based on Parker Solar Probe (PSP) and Solar Orbiter data at various distances from the Sun, we show the general trends and compare them with Wind observations near 1 au. The paper analyzes solar wind power spectra of magnetic field fluctuations in the inertial and kinetic ranges of frequencies. We find a systematic steepening of the spectrum in the inertial range with the spectral index of around $-3/2$ at closest approach to the Sun toward $-5/3$ at larger distances (above 0.4 au), the spectrum of the field component perpendicular to the background field being steeper at all distances. In the kinetic range, the spectral indices increase with distance from -4.8 at closest PSP approach to ≈ -3 at 0.4 au and this value remains approximately constant toward 1 au. We show that the radial profiles of spectral slopes, fluctuation amplitudes, spectral breaks, and their mutual relations undergo rapid changes near 0.4 au.

Unified Astronomy Thesaurus concepts: Solar wind (1534)

1. Introduction

The solar wind is a turbulent plasma (e.g., Alexandrova et al. 2013; Bruno & Carbone 2013; Chen 2016, for overview) that emanates from the solar corona and carries the frozen-in magnetic field into the heliosphere. Turbulent solar wind fluctuations are characterized by a broad power spectrum that covers timescales from several hours to about 0.01 s in the spacecraft reference frame (e.g., Coleman 1968; Alexandrova et al. 2013). Observations at different distances from the Sun show that the solar wind expansion is nonadiabatic and a turbulent cascade is considered to be one of the important sources of energy for this nonadiabatic behavior. The turbulent cascade transfers the energy from an outer energy containing scale over the inertial range to the ion gyroscale. Below the ion gyroscale, a new mode of turbulence carries energy to yet smaller scales where it is dissipated (Alexandrova et al. 2008; Sahraoui et al. 2009; Schekochihin et al. 2009).

In the inertial range, the power spectra of the magnetic field are generally interpreted in terms of magnetohydrodynamic (MHD) turbulence theory (e.g., Matthaeus & Goldstein 1982; Goldreich & Sridhar 1995; Galtier et al. 2000; Schekochihin et al. 2009). The magnetic fluctuations are predominantly perpendicular to the local mean magnetic field direction and the spectral index at 1 au is close to $-5/3$ (e.g., Matthaeus & Goldstein 1982; Bale et al. 2005; Chen et al. 2011). At the small-scale end of the inertial range, the magnetic energy spectrum steepens and below the transition range, the polarization properties of turbulence resemble those of kinetic Alfvén waves (Bale et al. 2005; Chen et al. 2013). At these kinetic scales, the spectral index of the fluctuations is typically between -2 and -4 (e.g., Leamon et al. 1998; Bale et al. 2005; Alexandrova et al. 2009; Chen et al. 2013; Chen 2016) in near-Earth space.

The majority of the aforementioned results refer to measurements around 1 au where turbulence is well developed and external forcing is negligible for most of the time. Parker Solar Probe (PSP) for the first time visited regions close to the Sun where turbulence is born and its observations are thus of great interest and intensively analyzed. Using a radial alignment between PSP and Solar Orbiter (SolO), Telloni et al. (2021) discuss the evolution of the plasma from a highly Alfvénic, less-developed turbulence state near the Sun to fully developed and intermittent turbulence at 1 au and conclude that their observations provide strong evidence for the radial evolution of the solar wind turbulence. Duan et al. (2021) use the first PSP encounter to study turbulence anisotropy at kinetic scales. They find a steepening of the power spectra with increasing angle between the background magnetic field and the solar wind velocity. Bowen et al. (2020) report very steep power spectra just above the ion-kinetic scales, similar to previous observations at 1 au, with a power-law index of near -4 at a spacecraft-frame frequency of about ≈ 4 Hz. The authors discuss two possible mechanisms leading to the observed spectral steepening: (1) the intensive dissipation at the considered range of frequencies, and (2) the significant decrease of characteristic nonlinear interaction times comparing with the expectation based on the dispersive nature of nonlinearly interacting kinetic Alfvén waves. They conclude that a further analysis including electric field fluctuations is required to elucidate this problem.

Chen et al. (2020) investigate the behavior of the power spectral density (PSD) at different heliocentric distances in the inertial range using the first two orbits of PSP, showing the spectral index transitions from $-3/2$ to $-5/3$ when passing from 0.17 au to 0.6 au. Similar results obtained by Shi et al.

(2021) focus on the inertial range of frequencies and report a steepening of the magnetic power spectra in the inertial range from −1.55 close to the Sun to −1.68 at larger distances. Zhao et al. (2020) analyze spectral features of turbulence in the field aligned solar wind and argue that PSP magnetic field observations are consistent with the predictions of nearly incompressible MHD theory and exhibit a $-5/3$ power-law index.

The results of these first studies are based on several cases and/or small statistics. We use all publicly available PSP and SolO observations of the magnetic field vector to date and analyze the evolution of the PSDs of compressive, $B_{\parallel}$ and noncompressive, $B_{\perp}$ fluctuations through the range of heliocentric distances covered by PSP and SolO. We compare these results with a similar analysis of Wind observations at 1 au, focusing predominantly on the kinetic range.

2. Data: Sources and Characterization

We use data from the first nine orbits of PSP covering the time between 2018 October 31 and 2021 September 30, combine them with SolO measurements between 2020 June 23 and 2022 January 30, and compare with Wind observations in the periods for which PSP and SolO data are available. The basic properties of the turbulence are thus investigated down to a distance of 0.12 au from the Sun, along with their radial evolution out to ≈1 au.

We use PSP magnetic field data (with a time resolution of 128 or 256 Hz) from the MAG fluxgate magnetometer, a part of the FIELDS instrument suite (Bale et al. 2016). Plasma parameters used for the computation of proton β (the ratio of the thermal pressure, $p_{\rm th} = nkT$ to the magnetic pressure, $p_{\rm mag} = B^2/2\mu_0$, where n and T are the proton density and temperature, k is the Boltzmann's constant, B is the background magnetic field strength, and μ_0 is vacuum permeability) are derived from the Solar Probe Cup of the SWEAP suite (Case et al. 2020). The SolO magnetometer (Horbury et al. 2020) measurements (with a time resolution of 64 and 128 Hz) cover distances from ≈0.5 to 1 au from the Sun. This data set is complemented with Wind magnetic field and plasma measurements at 1 au (plasma data cadence ≈98 s and magnetic field resolution 10 Hz, Lepping et al. 1995 and Ogilvie et al. 1995). Our data set contains a total of 524,036 20 minute partly overlapping time intervals; 327,334 and 70,077 from SolO with a time resolution of 64 and 128 Hz, respectively, and 126,625 time intervals from PSP at different distances from the Sun. The same number of Wind time intervals is added for a comparison. We use full time resolution data but the study is limited to 5 Hz to be comparable with the Wind measurements.

We describe the fluctuation amplitudes by the standard deviation, σB computed over our intervals. We use the standard deviation of the perpendicular component, $B_{\perp}$ as a proxy of the amplitude of the noncompressive fluctuations and the standard deviation of the magnetic field strength, $|B| \approx B_{\parallel}$ for a proxy of the amplitude of compressive fluctuations (Šafránková et al. 2015) but we note that the PSD of $|B|$ includes also pressure balanced structures or magnetic holes. The reason for this approach is the potential overestimation of PSD $B_{\parallel}$ due to inaccuracies in the determination of the local parallel direction when the vector fluctuation level is comparable with the background magnetic field. For the same reason, we limit the study of turbulence properties in the kinetic range to the trace PSDs.

The blue line in Figure 1(a) shows the estimated profile of the magnetic field strength, $B(r)$. We use a standard model for the Parker spiral in the solar equatorial plane, fulfilling the following equation:

$$B(r) = B(r_0) \cdot (r_0/r)^2 \cdot (1 + (\Omega/V_{\rm SW})^2 \cdot (r - r_0)^2)^{\frac{1}{2}} \quad (1)$$

where the constants $r_0 = 0.1$ au, $B(r_0) = 250$ nT (the magnetic field at r_0), the solar wind velocity, $V_{\rm SW} = 325$ km s^{-1}, and the solar angular velocity, $\Omega = 2.9 \times 10^{-6}$ s^{-1} are chosen to match the PSP observations at its closest approach. The figure demonstrates that the average values of the magnetic field strength follow very well the Parker prediction from 0.1 au through 1 au to the Mars orbit (two additional red points at ≈1.5 au). The magnetic field data for these points are taken from the MAG instrument (Connerney et al. 2015) on board the Mars Atmosphere and Volatile Evolution (MAVEN) spacecraft.

The dependence of proton β on the distance from the Sun in Figure 1(b) (only data from PSP) shows that the median β starts from a value of 0.1 near the Sun (≈.0.1 au) and gradually increases to ≈0.35 at 0.3 au and similar values are observed at even larger distances. The blue horizontal line represents the median β at 1 au (≈0.35, Wind data) and this value is consistent with the trend observed by PSP. The agreement is not perfect but it should be taken into account that PSP and Wind are regularly located at different longitudes and thus in solar wind streams coming from different source regions even when measurements from the same time intervals are combined.

The main goal of our analysis is to demonstrate the evolution of the turbulent spectra in the inner heliosphere, i.e., to quantify their development with distance from the solar wind source region. However, the magnetic field strength decreases nearly by 2 orders of magnitude through the investigated range of distances and so does the fluctuation amplitude as the spread of points in Figure 1(a) suggests. Since the amplitude of the fluctuations is one of the factors that affects the shape of the PSD (e.g., Šafránková et al. 2015, 2016), the next four panels in Figure 1 analyze its radial evolution. The medians of particular quantities at 1 au computed from the Wind data are added as blue horizontal lines to the corresponding panels. Note that the medians discussed throughout the paper are medians of particular quantities even when the scales in the plots are logarithmic.

The amplitude of the compressive fluctuations (Figure 1(c)) is smaller than that of the noncompressive fluctuations (Figure 1(d)) but this difference decreases with distance from the Sun. Whereas it is 1 order of magnitude at 0.1 au it is only a factor of 3 at 0.4 au and beyond to 1 au. Since the background magnetic field decreases faster (Figure 1(a)), the normalized amplitude of the compressive fluctuations, $(\sigma|B|)/|B|$ (Figure 1(e)), increases with distance from the Sun until about 0.3 au where it reaches a value of 0.03 that is close to that observed by Wind. This trend is consistent with findings of van der Holst et al. (2022) although these authors analyze only one event. The normalized level of noncompressive fluctuations, $(\sigma B_{\perp})/|B|$ (Figure 1(f)), is approximately constant all the way from 0.3 to 1 au. We attribute the weak decreasing trend quantified by the correlation coefficients at the top of the figure to the gradual dissipation of turbulence that heats the solar wind.

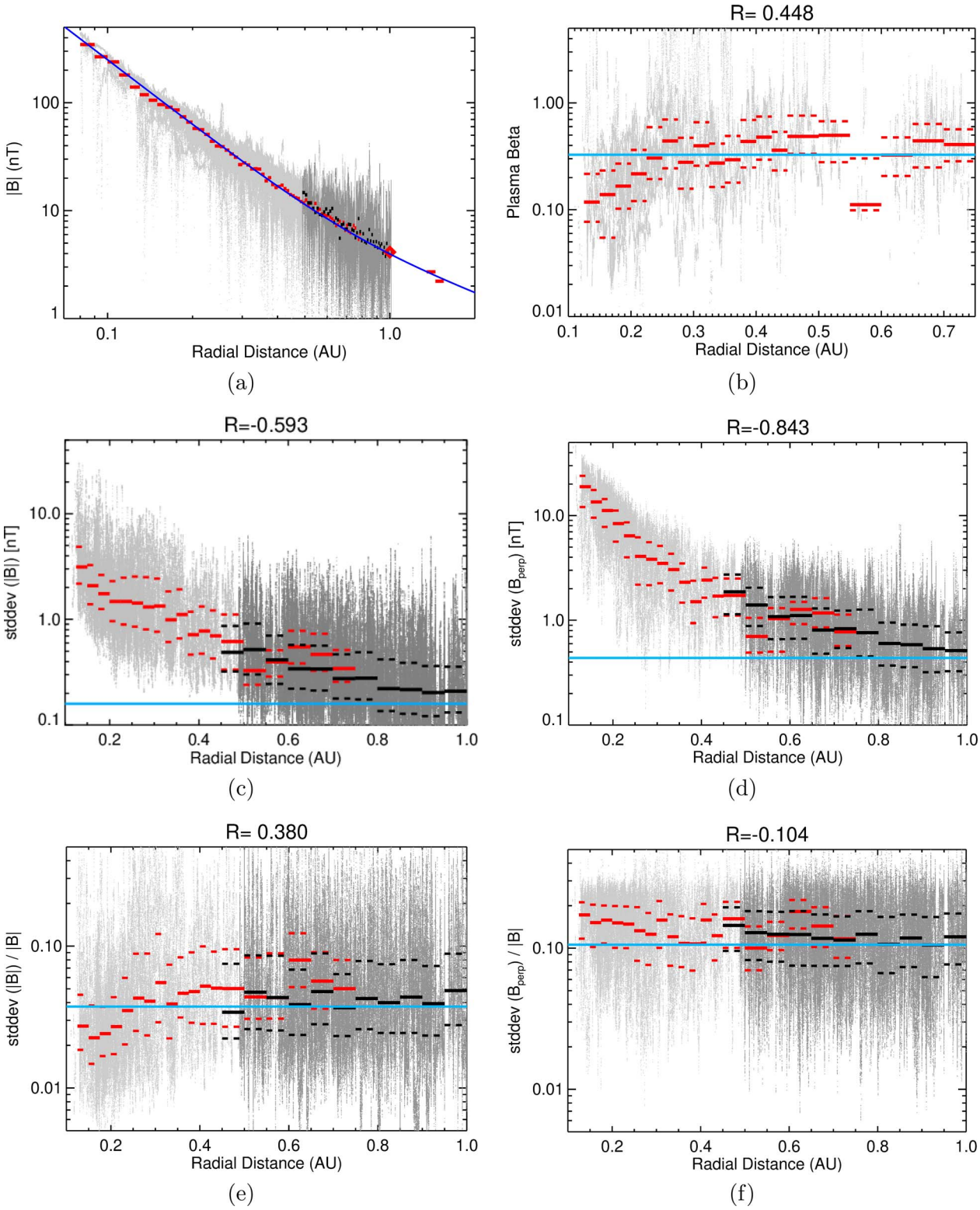

Figure 1. Evolution of (a) the magnetic field strength, $|B|$; (b) proton β; (c) the standard deviation of the magnetic field strength, $\sigma|B|$; (d) the standard deviation of the perpendicular magnetic field component, $\sigma B_{\perp}$; (e) normalized $\sigma|B|/|B|$; and (f) normalized $\sigma B_{\perp}/|B|$ with distance from the Sun. Gray dots represent the values of each quantity averaged over a given 20 minute interval (light and heavy gray points show PSP and SolO intervals, respectively); full red (PSP) and black (SolO) bars show the standard deviation medians in distance bins; and dashed red and black bars show their first and third quartiles. The Spearman correlation coefficients are given on top of each panel. The light blue horizontal lines represent the median value of a particular parameter at 1 au determined from the Wind data.

3. Average PSDs in the Inertial Range at Different Distances

The standard deviations of the magnetic field measured by PSP and SolO (Figure 1) show a clear decreasing level of compressive (Figure 1(c)) as well as noncompressive (Figure 1(d)) magnetic field fluctuations with distance from the Sun. The same trend is observable in the top panels of Figure 2, which show median PSDs of both compressive

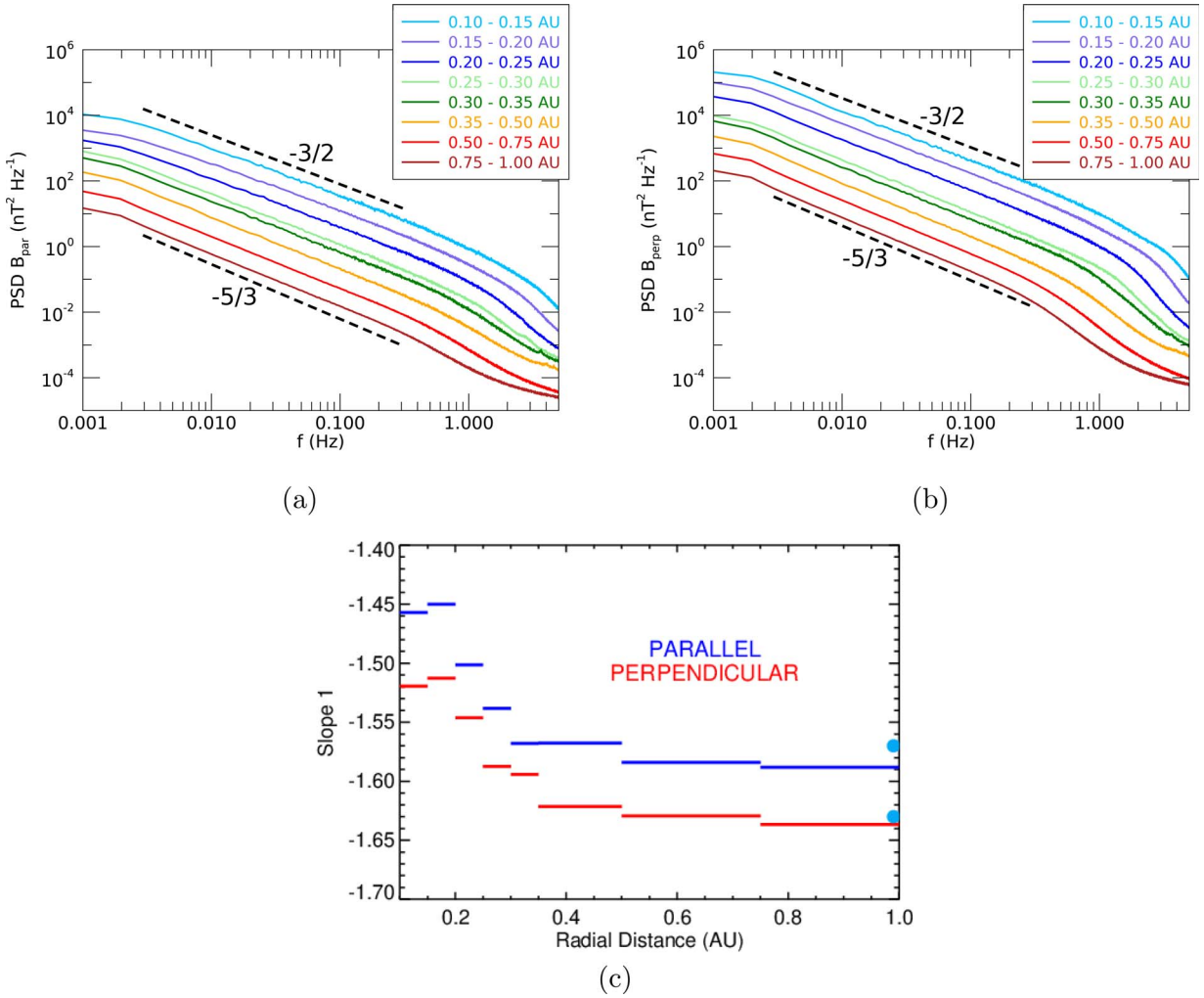

Figure 2. Median PSD spectra of (a) compressive and (b) noncompressive magnetic field fluctuations in different distance bins from the Sun (in the spacecraft frame); (c) Variations of the magnetic field spectral index as a function of heliocentric distance in the inertial range (10^{-2}–10^{-1} Hz). The light blue points indicate the values of the slopes in the large statistics of Wind data (Šafránková, 2019).

(Figure 2(a)) and noncompressive (Figure 2(b)) magnetic field fluctuations binned by distance from the Sun. The figure combines both PSP and SolO data and the PSD is calculated by a fast Fourier transform (Šafránková et al. 2015) of the 20 minute subintervals. We apply the Hanning window and linearly interpolate data gaps. To achieve the smooth profiles that are shown in Figure 2, we use two-step averaging. We apply overlapping of 19 minutes for the basic subintervals and this approach significantly increases the number of spectra for consecutive averaging; each of the PSDs in the figure is computed as the median of 5000 or more individual spectra.

In the inertial range, the power of the $B_\perp$ fluctuations (Figure 2(b)) is by a factor of 20 greater than that of the $B_\parallel$ fluctuations (Figure 2(a)) in all distance bins. The top panels reveal that the spectral index changes from $-3/2$ to $-5/3$ when moving away from the Sun. Figure 2(c) shows the slopes of the PSDs determined by fits in the frequency range between 10^{-2} and 10^{-1} Hz as a function of distance from the Sun. The median frequency spectra of the compressive fluctuations are shallower than those of noncompressive fluctuations but both slopes exhibit similar decreasing trends until ≈0.35 au. The PSD slopes of both types of fluctuations are approximately constant beyond 0.35 au and equal to those at 1 au (Wind). The evolution of the spectral slope is consistent with already published trends (Chen et al. 2020; Alberti et al. 2022); however, our averaging of a large number of spectra reveals a clear feature; the spectral slopes steepen until ≈0.35 au and remain constant beyond this distance.

4. Spectral Slope in the Kinetic Range of Frequencies

The median spectra show a steepening of the spectral slope near the ion spectral break (further called the kinetic range) toward the Sun. However, this evolution cannot be quantified from the median spectra because the slope can be affected by the magnetometer noise at larger distances (Pitňa et al. 2021) and the part of the spectrum following the break is too short for a reliable fitting closer to the Sun. Therefore, we use the local slope determined from a full magnetic field vector which is calculated as follows. The spectrum in the interval $\langle f_i, 2f_i \rangle$ is fitted with a straight line, and its direction is attributed to the center frequency of the given interval. The frequency f_i starts at 0.1 Hz and increases in steps of 0.01–5 Hz. The steepest slope of the interval is considered the local spectral slope in the kinetic range and denoted as slope 2 in the following figures.

We also record the frequency f_j corresponding to the interval $\langle f_j, 2f_j \rangle$ in which we take the frequency of the minimum slope as a proxy for the location of the spectral break, $f_{\min}$. Its profile is shown in Figure 3(a) as an illustration of the break shifting with the distance from the Sun. The $f_{\min}$ frequencies are shown with gray (PSP) or black (SolO) dots. The red (PSP) or black (SolO) bars represent the medians, the dotted lines show the first and third quartiles.

Bruno & Trenchi (2014) investigate the radial dependence of the spectral break separating the inertial from the kinetic range in PSDs of magnetic field fluctuations between 0.42 and 5.3 au. They find that the spectral break moves to higher frequencies as the heliocentric distance decreases. They give the dependence of the break frequency, f_b, on the distance from the Sun R in the spacecraft frame as $f_b = 0.32 \times R^{-1.08}$, which is shown as a green line in Figure 3(a). Our profile distinguished by medians in distance bins is similar at the overlapping distances (≈0.4 au and beyond) but a much steeper increase of the $f_{\min}$ frequency is observed closer to the Sun. Since a comparison with Figure 1(a) reveals that the scaling roughly corresponds to $1/|B|$, we add the proton gyro-frequency as a blue line to the panel in order to show this trend. We note that a deeper discussion of the spectral break behavior would require the application of Taylor's hypothesis, recalculation of the spectra into k-vector space, and a more precise break determination that is out of the scope of the present paper.

Figure 3(b) presents PSD slope 2 as a function of the radial distance. The color coding follows Figure 3(a). The light blue horizontal line presents the median value of spectral slope 2 at 1 au as identified in the Wind data. Slope 2 quickly increases from −4.8 near the Sun to a value around −3, which corresponds to the Wind and SolO measurements closer to 1 au. The figure highlights again the distance of around 0.4 au where the trend changes.

The last four panels in Figure 3 show statistical dependencies of slope 2 with the level of compressive and noncompressive fluctuations. The format of these panels is the same as that of the previous ones. The large light blue dots mark the median slopes determined at 1 au from Wind magnetic field measurements for comparison. Figures 3(c) and 3(e) show similar and established trends of the spectral steepening with an increasing level of compressive (Figure 3(c)) or noncompressive (Figure 3(d)) fluctuations. Šafránková et al. (2015) quantify the level of fluctuations by their standard deviations and their relation to spectral slopes. They demonstrate that the spectrum becomes steeper in a more disturbed flow in both the inertial and kinetic ranges. A similar steepening in the kinetic part of the spectrum with increasing fluctuation level is also reported by Bruno et al. (2014b) for magnetic field fluctuations.

Median values determined from data of the different spacecraft at a very low level of fluctuations suggest that the spectra in the kinetic range are shallower close to the Sun for the same level of fluctuations and this trend coincides with the flattening of the spectra in the inertial range (Figure 2). However, the level of fluctuations strongly depends on the distance from the Sun (Figure 1), and thus the ranges of fluctuations determined for our three spacecraft overlap only partly. The principal reason for the decrease of the magnetic field strength and fluctuation amplitude is the solar wind expansion. Although the expansion is an important factor for the development of the turbulence in the solar wind and some experimentally determined features cannot be reproduced by models if it is not included (Grappin et al. 2022), the expansion alone cannot change the character of turbulence because the fluctuations decrease with the same rate as the magnetic field magnitude. It implies that their normalized level would be conserved.

For this reason, Figures 3(e) and (f) present slope 2 as a function of the normalized levels of compressive and noncompressive fluctuations. Whereas the level of compressive fluctuations does not influence the PSD slope at 0.5–1 au significantly (SolO and Wind profiles are nearly equal), we observe a strong flattening of the spectra in the PSP data (Figure 3(e)) with increasing fluctuation level. On the other hand, increasing of the noncompressive fluctuation level leads to steeper spectra at all distances. In accord with Šafránková et al. (2015), we propose that the spectral steepening with an increasing level of fluctuations can be connected with the decreasing effectiveness of the processes responsible for the cascading of turbulent energy to shorter scales due to nonlinear effects if the fluctuations are large.

The combination of all panels suggests that the mechanisms shaping the spectra at PSP distances and in the distance range between 0.5 and 1 au can be different. Figure 3(b), as well as Figures 1(a), 1(d), (e) and Figure 2(c), points at the existence of a "critical boundary" located at around 0.3–0.4 au. We investigate this point further in the next section.

5. Spectral Slope 2 in Two Ranges of Distances from the Sun

We have divided our observations into two subsets according to the distance from the Sun. The left panels in Figure 4 present the data gathered at 0.1–0.3 au (PSP data only) and the right-hand panels in Figure 4 present the data of PSP and SolO at distances 0.4–1 au (we skipped the distance bin 0.3–0.4 au to highlight the differences between the left and right panels). The trends observed at 1 au are given in all panels (Wind, light blue dots). The value of PSD slope 2 and its dependence on the fluctuation amplitude determined from PSP and SolO measurements at larger distances (Figures 4(b), (d)) is generally close to the trends observed at 1 au. It is important to note that not only median slopes but also the width of distributions in all bins shown by the dotted lines of corresponding color are very similar for the PSP and SolO data sets. By contrast, the dependence of slope 2 on the fluctuation amplitudes close to the Sun follows an opposite trend to the trends determined at 1 au. The power exponents become very similar to those at 1 au only for the highest normalized levels of both compressive and noncompressive fluctuations (Figures 4(a), (c)).

6. Summary and Conclusion

We present our investigation of the evolution of the magnetic field fluctuations in the inner heliosphere based on PSP, SolO and Wind observations over a total time of 3 yr. The first part of our analysis concentrates on the radial evolution of the amplitude of the magnetic field fluctuations that is expected

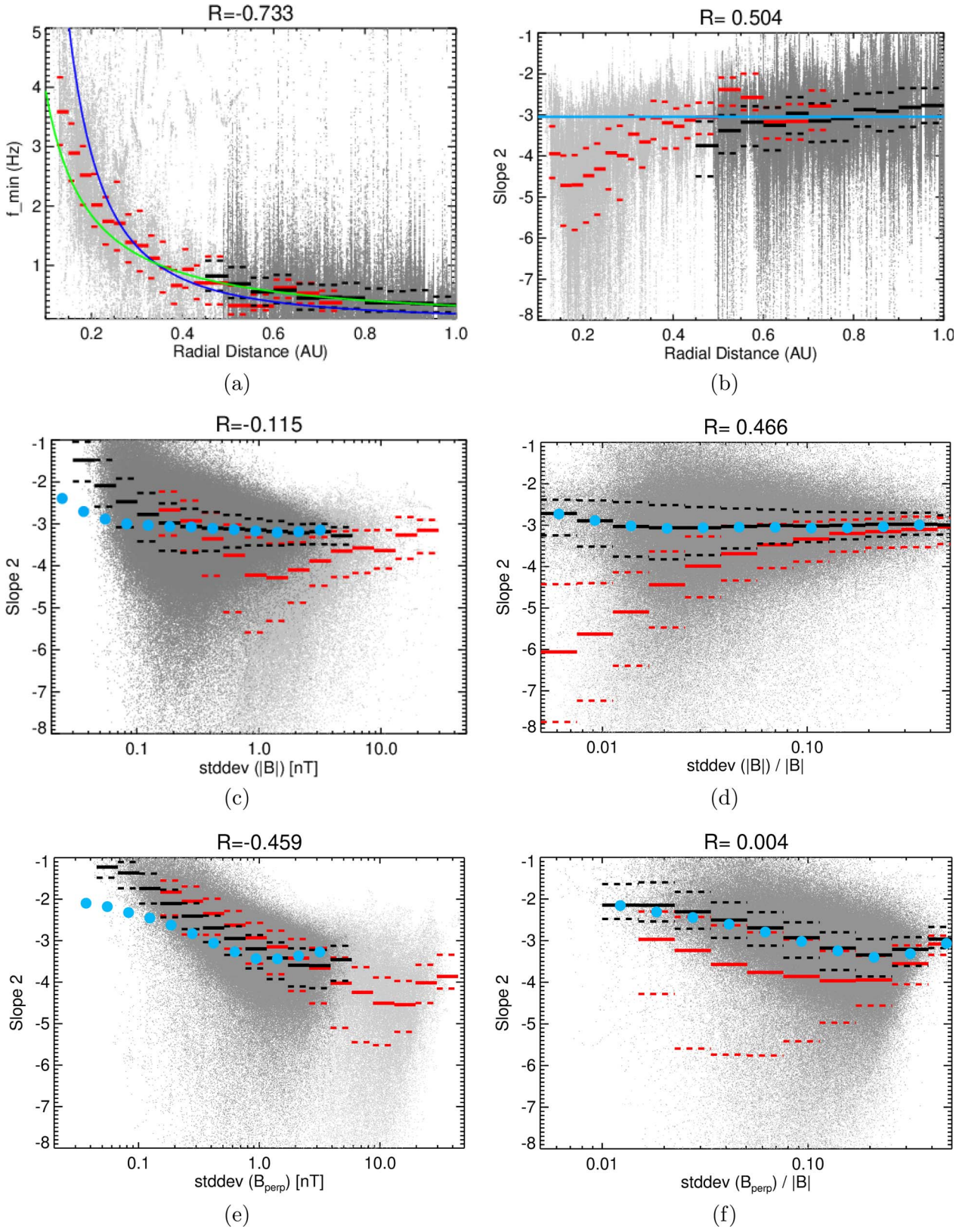

Figure 3. (a) Dependence of the $f_{\rm min}$ frequency as a proxy of the ion spectral break; and (b) PSD slope 2 of $|B|$ fluctuations in the kinetic range for different distance bins. PSD slope 2 as a function of: (c) $\sigma|B|$, (d) $\sigma|B|$ normalized to background $|B|$; (e) $\sigma B_{\perp}$, and (f) $\sigma B_{\perp}$ normalized to $|B|$. The format follows Figure 2, the light blue dots in all panels and the horizontal line in the panel (b) show medians of slope 2 determined from Wind observations at 1 au.

to control the PSD shape and contributes to solar wind heating in the inner heliosphere. The basic results shown in Figure 1 can be summarized as follows:

1. The median magnetic field strength decreases by 2 orders of magnitude from 0.1 to 1 au (and beyond) and follows roughly the Parker spiral prediction.

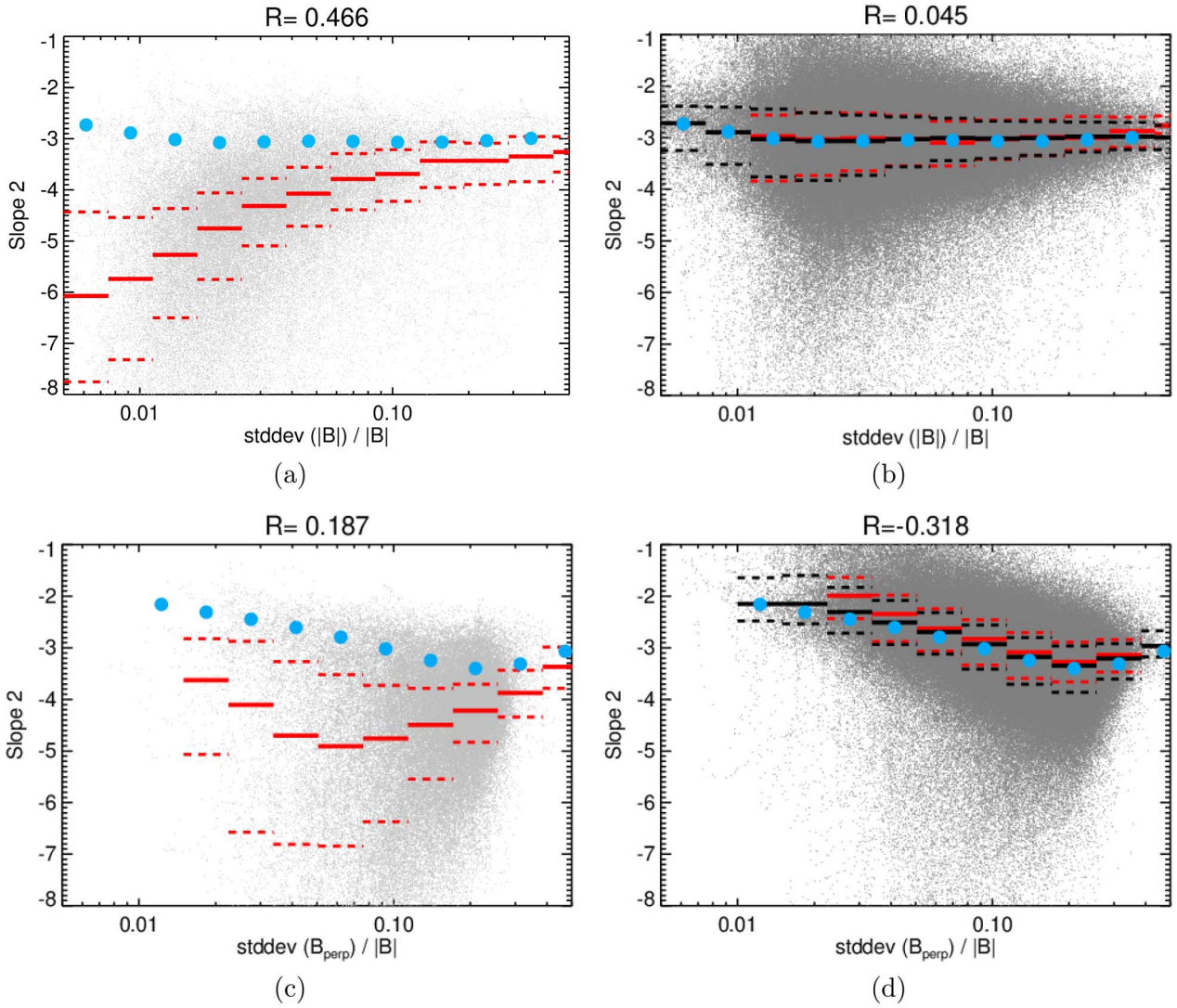

Figure 4. PSD slope 2 in two distance ranges. The left panels show PSP data (red) at distances between 0.1 and 0.3 au; the right panels show PSP data (red) and SolO data (black) at distances between 0.4 and 1 au. We overplot Wind data at 1 au for reference on all panels. The slopes are shown as a function of: (a, b) $\sigma|B|$ normalized to the background value of $|B|$; and (c, d) $\sigma B_\perp$ normalized to $|B|$.

2. The median proton β increases from $\approx$0.1 at 0.1 au to $\approx$0.4 at $\approx$0.3 au and then becomes constant until 1 au.
3. The level (standard deviation) of compressive as well as noncompressive magnetic field fluctuations decreases with distance from the Sun at approximately the same rate as the decreasing magnitude of the magnetic field.
4. The level of noncompressive fluctuations normalized to the average magnetic field strength weakly decreases with radial distance, whereas the normalized level of compressive fluctuations increases with distance until $\approx$0.4 au, beyond which is stays nearly constant.

Our analysis of the PSD evolution in the inertial range (Figure 2) shows the following:

1. A general steepening of the magnetic field spectral index from $-3/2$ to $-5/3$, as reported by Chen et al. (2020), Bowen et al. (2020), Shi et al. (2021), and Lotz et al. (2023). The observed PSDs of the noncompressive fluctuations are always steeper than the PSDs of the compressive fluctuations.
2. The steepening of the spectra ends approximately at $\approx$0.4 au as pointed out by Alberti et al. (2022) and observed by Lotz et al. (2023).
3. Beyond $\approx$0.4 au, the power exponents remain approximately constant and equal to the 1 au level determined from Wind data (e.g., Šafránková 2019).

Our study of the radial dependence of the spectral parameters in the kinetic range (Figure 3) indicates that

1. Our proxy of the break frequency between the inertial and kinetic ranges decreases with distance approximately as $1/|B|$ below 0.4 au, i.e., it follows roughly the change of the gyroradius (blue line in Figure 3(a)).
2. The decrease of the break frequency with distance is slower beyond 0.4 au and follows the trend found by Bruno & Trenchi (2014). We note that similar dependencies are shown by Duan et al. (2020) and Lotz et al. (2023).
3. The median value of slope 2 increases from a value between -5 and -4 (Bowen et al. 2020; Franci et al.

2020) close to the Sun (if the magnetic field fluctuations are small) to a value around −2.8 at 0.4 au and beyond. A similar value is found by Šafránková (2019) and explained by the interplay of Alfvénic and slow-mode fluctuations.

Finally, the separation of the data set into two subsets (Figure 4) reveals that

1. Slope 2 is well ordered by the normalized amplitude of the compressive and noncompressive fluctuations and increases with this level from −6 for very low fluctuation amplitudes to about −3.6 below ≈0.4 au. It only slightly decreases with the fluctuation amplitude beyond 0.4 au where all analyzed data sets (PSP, SolO, Wind) exhibit identical slightly decreasing trends of slope 2 toward the value of −2.8 (e.g., Chen et al. 2013).

Our study demonstrates how turbulence in the inner heliosphere evolves with radial distance from the Sun. Our data set contains many different structures like corotating interaction regions, coronal mass ejections, switchbacks or reconnection exhausts and does not differentiate latitudes and longitudes of the spacecraft. Nevertheless, the robust statistics based on more than 550,000 individual intervals shows that PSP and SolO data complement each other very well and that the observed radial trends of median values of all investigated parameters reach those determined at 1 au from the Wind data (Figures 4(b), (d)). Our study emphasizes the importance of the region between ≈0.1 and 0.4 au for the development of turbulence in both frequency ranges.

We conclude that the evolution of turbulence is apparently controlled by different processes close to the Sun (below ≈0.4 au) and at larger distances. The solar wind expansion lowers the magnetic field fluctuation amplitudes significantly but conserves their normalized level, and compressibility as well as the median values of the PSD slopes in the inertial and kinetic ranges because the nonlinear interactions have enough time to set up fully developed turbulence. The shape of the PSDs is formed by the cascading of energy from larger to smaller scales and can be understood using standard theories (Telloni et al. 2021, and references therein).

In spite of expansion, the normalized level of compressive magnetic field fluctuations at distances below 0.35 au increases with distance and turbulence changes its character from Alfvén-like near the Sun to a fully developed state beyond 0.4 au (see e.g., Telloni et al. 2021; Alberti et al. 2022). Since PSP orbits at streamer belt latitudes, it is possible that reconnection of closed field lines of coronal loops with open field lines from neighboring coronal holes serves as an additional source of fluctuations. This interpretation is consistent with the increasing occurrence rate of switchbacks (Macneil et al. 2020; Tenerani et al. 2021) if switchbacks are produced by this type of interchange reconnection (Sterling & Moore 2020). This process adds fluctuation energy to larger scales and thus the corresponding part of the turbulent spectrum is shallower. However, the fluctuations in the kinetic range behave in the opposite way closer to the Sun and at larger distances if plotted as a function of the fluctuation amplitude. Whereas the steepening of the spectra with fluctuation amplitude at larger distances can be connected with the saturation of the cascade rate, the spectral flattening observed closer than ≈0.35–0.4 au from the Sun requires understanding how the turbulent fluctuations are born in the distant corona. One can only speculate whether the coincidence of this critical boundary with the altitude where the negative tangential component of the solar wind velocity peaks (Němeček et al. 2020) is random or whether it is related to the same process.

A separation of the data from our set according to different solar wind types (fast, slow, slow Alfvénic), magnetic field orientations (radial versus Parker spiral orientation), or regions (corotating interaction/rarefaction regions, coronal mass ejections) will be the first step of further investigations. We also plan to elucidate mutual relations of the magnetic field and velocity fluctuations and to discuss the influence of the parameters describing the plasma state, like the plasma beta or temperature anisotropy. All these studies require recalculation of the data to the plasma frame to account for changing solar wind velocity.

The authors thank all PSP, SolO, and Wind spacecraft teams for the plasma and magnetic field data. All used data are from open-access sources via (http://cdaweb.gsfc.nasa.gov/cdaweb/). D.V. is supported by STFC Ernest Rutherford Fellowship ST/P003826/1 and STFC Consolidated Grants ST/S000240/1 and ST/W001004/1. The work of the Czech authors is supported by the Czech Science Foundation under Contracts 23-06401S and 22-10775S (F. N.).

Facilities: MAVEN, Parker Solar Probe, Solar Orbiter, Wind.

ORCID iDs

Jana Šafránková https://orcid.org/0000-0003-4178-5206
Zdeněk Němeček https://orcid.org/0000-0002-8160-3051
František Němec https://orcid.org/0000-0002-3233-2718
Daniel Verscharen https://orcid.org/0000-0002-0497-1096
Timothy S. Horbury https://orcid.org/0000-0002-7572-4690
Stuart D. Bale https://orcid.org/0000-0002-1989-3596
Lubomír Přech https://orcid.org/0000-0003-0867-0458

References

Alberti, T., Benella, S., Consolini, G., Stumpo, M., & Benzi, R. 2022, ApJL, 940, L13
Alexandrova, O., Carbone, V., Veltri, P., & Sorriso-Valvo, L. 2008, ApJ, 74, 1153
Alexandrova, O., Chen, C. H. K., Sorriso-Valvo, L., Horbury, T. S., & Bale, S. D. 2013, SSRv, 178, 101
Alexandrova, O., Saur, J., & Lacombe, C. 2009, PhRvL, 103, 165003
Bale, S. D., Goetz, K., Harvey, P. R., et al. 2016, SSRv, 204, 49
Bale, S. D., Kellogg, P. J., Mozer, F. S., Horbury, T. S., & Reme, H. 2005, PhRvL, 94, 21
Bowen, T. A., Mallet, A., Bale, S. D., et al. 2020, PhRvL, 125, 025102
Bruno, R., & Carbone, V. 2013, LRSP, 10, 2
Bruno, R., & Trenchi, L. 2014, ApJL, 787, L24
Bruno, R., Trenchi, L., & Telloni, D. 2014b, ApJL, 793, L15
Case, A. W., Kasper, J. C., Michael L. Stevens, M. L., et al. 2020, ApJS, 246, 43
Chen, C. H. K. 2016, JPlPh, 82, 535820602
Chen, C. H. K., Bale, S. D., Bonnell, J. W., et al. 2020, ApJS, 246, 53
Chen, C. H. K., Boldyrev, S., Xia, Q., & Perez, J. C. 2013, PhRvL, 110, 225002
Chen, C. H. K., Mallet, A., Yousef, T. A., Schekochihin, A. A., & Horbury, T. S. 2011, MNRAS, 415, 3219
Coleman, P. J. 1968, ApJ, 153, 371
Connerney, J. E. P., Espley, J., Lawton, P., et al. 2015, SSRv, 195, 257
Duan, D., Bowen, T. A., Chen, C. H. K., et al. 2020, ApJS, 246, 55
Duan, D., He, J., & Bowen, T. A. 2021, ApJL, 915, L8
Franci, L., Del Sarto, D., Papini, E., et al. 2020, arXiv:2010.05048v1

Galtier, S., Nazarenko, S. V., Newell, A. C., & Pouquet, A. 2000, JPlPh, 63, 447
Goldreich, P., & Sridhar, S. 1995, ApJ, 438, 763
Grappin, R., Verdini, A., & Müller, W.-C. 2022, ApJ, 933, 246
Horbury, T. S., O Brien, H., Blazquez, I. C., et al. 2020, A&A, 642, A9
Leamon, R. J., Smith, C. W., Ness, N. F., Matthaeus, W. H., & Wong, H. K. 1998, JGR, 103, 4775
Lepping, R. P., Acuna, M. H., Burlaga, L. F., et al. 1995, SSRv, 71, 207
Lotz, S., Nel, A. E., Wicks, R. T., et al. 2023, ApJ, 942, 93
Macneil, A. R., Owens, M. J., Wicks, R. T., et al. 2020, MNRAS, 494, 3642
Matthaeus, W. H., & Goldstein, M. L. 1982, JGR, 87, 6011
Němeček, Z., Ďurovcová, T., Šafránková, J. D., et al. 2020, ApJL, 897, L39
Ogilvie, K., Chornay, D., Fritzenreiter, R., et al. 1995, SSRv, 71, 55
Pitňa, A., Šafránková, J., Němeček, Z., Franci, L., & Pi, G. 2021, Atmos, 12, 1547
Šafránková, J., Němeček, Z., Němec, F., et al. 2015, ApJ, 803, 107
Šafránková, J., Němeček, Z., Němec, F., et al. 2016, ApJ, 825, 121
Safránková, J., Němeček, Z., Němec, F., et al. 2019, ApJ, 870, 40
Sahraoui, F., Goldstein, M. L., Robert, P., & Khotyaintsev, Y. V. 2009, PhRvL, 102, 231102
Schekochihin, A. A., Cowley, S. C., Dorland, W., et al. 2009, ApJS, 182, 310
Shi, C., Velli, M., Panasenco, O., et al. 2021, A&A, 650, A21
Sterling, A. C., & Moore, R. L. 2020, ApJL, 896, L18
Telloni, D., Sorriso-Valvo, L., Lloyd, D., et al. 2021, ApJL, 912, L21
Tenerani, A., Sioulas, N., & Matteini, L. 2021, ApJL, 919, L31
van der Holst, B., Huang, J., Sachdeva, N., et al. 2022, ApJ, 925, 146
Zhao, L.-L., Zank, G. P., & Adhikari, L. 2020, ApJ, 98, 113